Spatial redistribution of a globally constant marine biological carbon pump

Louise Delaigue

louise.delaigue@imev-mer.fr

Laboratoire d'Océanographie de Villefranche (CNRS-SU) https://orcid.org/0000-0002-9796-1128

Raphaëlle Sauzède

Sorbonne Université, CNRS, Institut de la Mer de Villefranche

Olivier Sulpis

CEREGE https://orcid.org/0000-0002-6463-3320

Philip Boyd

University of Tasmania https://orcid.org/0000-0001-7850-1911

Hervé Claustre

Sorbonne University / CNRS

Gert-Jan Reichart

Royal Netherlands Institute for Sea Research (NIOZ)

Matthew Humphreys

NIOZ Royal Netherlands Institute for Sea Research, Department of Ocean Systems (OCS), and Utrecht University https://orcid.org/0000-0002-9371-7128

Article

Keywords:

Posted Date: August 5th, 2025

DOI: https://doi.org/10.21203/rs.3.rs-7140275/v1

Additional Declarations: There is **NO** Competing Interest.

Spatial redistribution of a globally constant marine biological carbon pump

L. Delaigue[1,2], R. Sauzède[3], O. Sulpis[4], P. W. Boyd[5], H. Claustre[2], G-J. Reichart[1,6] and M. P. Humphreys[1]

[1]Department of Ocean Systems (OCS), NIOZ Royal Netherlands Institute for Sea Research, PO Box 59, 1790 AB Den Burg (Texel), the Netherlands

[2]Sorbonne Université, CNRS, Laboratoire d'Océanographie de Villefranche, Villefranche-Sur-Mer, France

[3]Sorbonne Université, CNRS, Institut de la Mer de Villefranche, Villefranche-Sur-Mer, France

[4]CEREGE, Aix Marseille Univ, CNRS, IRD, INRAE, Collège de France, Aix-en-Provence, France

[5]Institute for Marine and Antarctic Studies, University of Tasmania, Hobart, Tasmania, Australia

[6]Department of Earth Sciences, Utrecht University, Utrecht, the Netherlands

Corresponding author: Louise Delaigue (louise.delaigue@imev-mer.fr)

Abstract

Marine dissolved inorganic carbon (DIC_{total}) is a key component of the global ocean carbon cycle. Over recent decades, DIC has increased due to rising anthropogenic CO_2, but the component of DIC change due to the biological carbon pump (BCP), which transfers carbon from the surface to the deep ocean, remains highly uncertain. Using the GOBAI-O_2 data product and the CANYON-B and CONTENT algorithms, we reconstructed the 3-dimensional global DIC_{total} distribution from 2004 to 2022 and decomposed it into DIC_{soft} (organic matter degradation), DIC_{carb} (carbonate dissolution), and DIC_{anth} (anthropogenic CO_2). We found a significant DIC_{total} change throughout the water column, with surface concentrations increasing by ~1.0 ± 0.23 µmol kg^{-1} yr^{-1}, driven by DIC_{anth} (>90% contribution). Despite a globally constant signal in DIC_{soft}, substantial regional trends emerged. Changes in circulation, particle sinking, and remineralization altered the vertical and horizontal distributions of DIC_{soft}. In some regions, DIC_{soft} accumulated at shallower depths, shortening residence times; in others, it was transported deeper, enhancing long-term storage. Although these widespread and divergent trends had little net effect on the global DIC_{soft} inventory from 2004-2022, the emerging spatial reorganization of the BCP may signal an evolving instability in the ocean carbon sink under continued climate forcing.

Main text

The ocean is a major CO_2 reservoir and sink. It holds ~37,000 GtC of dissolved inorganic carbon (DIC)—40 times more than the atmosphere (Siegenthaler & Sarmiento, 1993; Friedlingstein et al., 2025). Anthropogenic CO_2 emissions, projected to increase by ~50% by 2050 relative to present levels (Masson-Delmotte et al., 2021), drove the accumulation of dissolved inorganic carbon (DIC) in seawater at a rate of ~3.2 ± 0.7 GtC per year from 2004 to 2019 (Keppler et al., 2023).

A major pathway for ocean carbon sequestration is the biological carbon pump (BCP), which transfers carbon from the surface to the ocean interior through two linked fluxes (Frenger et al., 2024). The *export flux* is the downward movement of biogenic carbon from the surface ocean (Dugdale & Goering, 1967; Boyd et al., 2019). The *return flux* involves the transformation of this exported carbon back into dissolved inorganic carbon (DIC), followed by its redistribution via ocean circulation.

The BCP is composed of two pumps which have opposite effects on marine CO_2 uptake from the atmosphere. The *soft tissue pump* removes DIC from the ocean surface through particulate organic carbon (POC) formation by marine phytoplankton. POC is then exported to depth, where it is eventually degraded by microbes and returned to DIC_{soft} (Volk & Hoffert, 1985). The respired DIC_{soft} that accumulates below the winter mixed layer constitutes the biologically sequestered carbon relevant to long-term climate regulation. The depth and residence time of this respired DIC_{soft} govern the BCP's climate impact (Kwon et al., 2009; Riebesell et al., 2009; Schlunegger et al., 2019; Frenger et al., 2024). The *carbonate counter-pump* influences DIC through carbonate formation in surface waters, which emits CO_2 by reducing alkalinity (Volk & Hoffert, 1985). As calcium carbonate particles sink and dissolve at depth, they release DIC_{carb} and alkalinity, neutralizing CO_2 (Feely et al., 2004; Sulpis et al., 2021). Therefore, the carbonate counter-pump opposes the soft tissue pump in its effect on marine CO_2 uptake from the atmosphere (Riebesell et al., 2009). Through this two-part sequence of processes of an export flux and a return flux, the BCP reduces atmospheric CO_2 by at least 163 ppm relative to a world without it (Tjiputra et al., 2025). The efficiency of the BCP depends mainly on the fraction of exported carbon that is sequestered in the return flux of the BCP as DIC_{soft}. This varies by region, and is influenced by ecosystem structure and functioning (driven by nutrients, temperature, light, and ocean stratification; Falkowski et al., 2000; Boyd & Trull, 2007), along with the combined effects of remineralization depth and water residence time in the ocean interior (Ricour et al., 2023).

Despite improved estimates of marine anthropogenic CO_2 uptake, uncertainties remain in its spatiotemporal variability and in the response of other DIC sources and sinks to environmental change (Gruber et al., 2023; Keppler et al., 2023). In particular, the response of the BCP to climate-driven change is still not well characterized. This gap is listed as a research priority for improving confidence in major Earth system processes assessed by the Intergovernmental Panel on Climate Change (IPCC; Pillar et al., 2024). Multiple interacting feedbacks, including changes in stratification, remineralization, particle dynamics, and ecosystem structure, can either amplify or dampen carbon sequestration (i.e. DIC_{soft}), with regionally divergent outcomes (Henson et al., 2022). The economic value of BCP-mediated sequestration has been placed at over US$900 billion per year (Berzaghi et al., 2025). Satellite data suggest a global increase in phytoplankton biomass in recent decades, though trends remain uncertain and spatially variable (Zhao et al., 2025). Likewise, the future BCP response remains uncertain, with Earth system models diverging on the

magnitude and direction of POC export changes across the 21st century, particularly at deeper, climate-relevant depth horizons (Henson et al., 2022; Walker & Palevsky, 2025).

The global inventory of DIC_{soft} has been considered relatively constant over recent decades compared to DIC_{anth} (Fig. 1; Gruber et al., 2023). However, studies suggest that since the late 20th century, POC export and the efficiency of DIC_{soft} sequestration have varied regionally, driven by shifts in circulation, nutrient supply, and plankton community structure (Humphreys et al., 2016; Fröb et al., 2018; Keppler et al., 2023; Delaigue et al., 2024). Recent observations show increasing DIC, with anthropogenic CO_2 driving gains near the surface and into intermediate depths, while DIC_{soft} appears to have been redistributed—from mid-latitudes to the tropics and from the surface to depth (>200 m)—without a net gain or loss in global total DIC_{soft}, based on the residual after subtracting DIC_{anth} from the total DIC inventory (Keppler et al., 2023). Climate-driven changes in circulation, nutrient supply, and plankton community composition may have led to regionally contrasting patterns in organic carbon export and sequestration of respired DIC_{soft} in the return flux of the BCP, shifting the geographic pattern of DIC_{soft} storage hotspots (Ciais et al., 2014; Henley et al., 2020; Lønborg et al., 2020; Bonino et al., 2021; Chaabane et al., 2024). This suggests that while the global magnitude of BCP-driven sequestration has not changed, its regional expression and sequestration efficiency are being reshaped by underlying climatic drivers, either independently or through shared regulating mechanisms.

Until now, it has been unclear whether this spatial reorganization of sequestered DIC_{soft} reflects true changes in BCP efficiency or a redistribution of DIC_{soft} driven by circulation changes. This has remained unsolved due to observational gaps in space and time. This uncertainty limits the ability to separate variability in DIC_{soft} sequestration from global trends and to evaluate the impact of the BCP on long-term marine carbon sequestration. One way to address this is by deriving DIC_{soft} (i.e., the respired and sequestered component of the soft tissue pump) directly from dissolved oxygen using Redfield stoichiometry, leveraging the global, high-resolution coverage of dissolved oxygen data from ship campaigns and BGC-Argo to enable spatiotemporally resolved assessments of biological carbon storage and emerging sequestration patterns (Redfield, 1958; Redfield, 1963; Anderson & Sarmiento, 1994).

In this study, we estimated 3D fields of DIC across space, time, and depth by applying the CANYON-B and CONTENT algorithms (Sauzède et al., 2017; Bittig et al., 2018) to the GOBAI-O_2 v2.1 product (Sharp et al., 2023). The resulting dataset, referred to as GCC-DIC (GOBAI-O_2 CANYON-B CONTENT-DIC), provides monthly DIC values on a 1° × 1° grid from 2004 to 2022, spanning 58 depth levels from 2.5 m to 1975 m (with higher resolution nearer the surface). We used this dataset to compute rates of total DIC change (ΔDIC_{total}), which we decomposed into its anthropogenic (ΔDIC_{anth}), biologically respired (ΔDIC_{soft}), and carbonate pump (ΔDIC_{carb}) components. To quantify BCP-driven DIC_{soft} sequestration, we calculated the accumulation and redistribution of DIC_{soft} below the winter maximum mixed layer depth (MLD) and integrated this down to 1975 m. For validation, we applied the same decomposition approach to a compilation of observational time series of carbonate chemistry from Lange et al. (2024). Additionally, we determined the depth at which 50% of the DIC_{soft} inventory was stored and assessed whether it deepened or shoaled over the study period, indicating changes in DIC_{soft} sequestration efficiency relevant to long-term climate feedbacks.

Global change in marine DIC

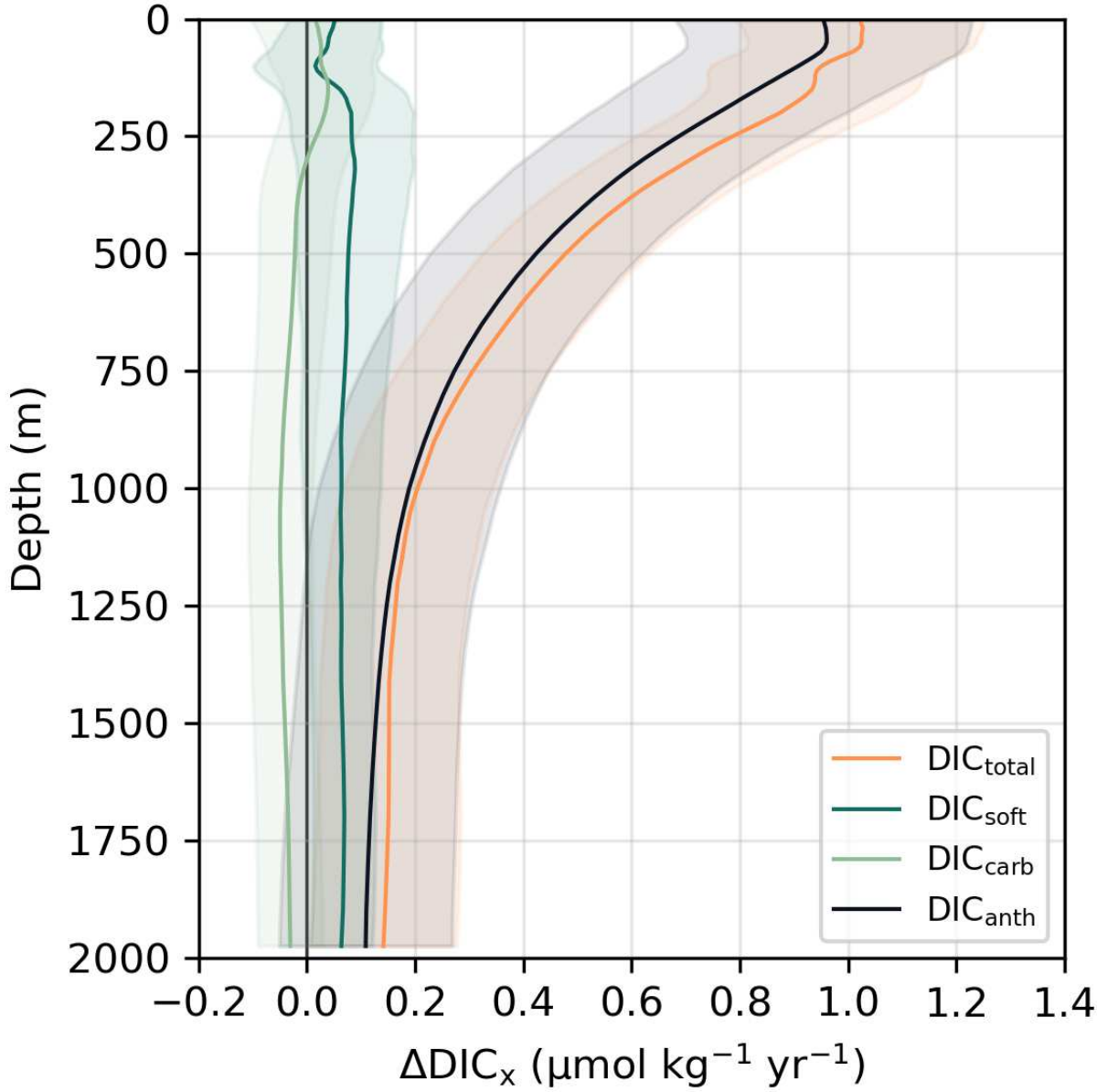

Figure 1. Global mean rates of change in each DIC component as a function of depth (m) within the upper 1975 m for the GCC-DIC dataset. Components include total DIC (DIC_{total}; orange), soft-tissue pump DIC (DIC_{soft}; green), carbonate pump DIC (DIC_{carb}; light green), and anthropogenic DIC (DIC_{anth}; black). These vertically resolved rates represent temporal changes in DIC concentrations per unit mass and form the basis for depth-integrated estimates shown in Figure 2. Shaded areas indicate ±1σ uncertainty. Vertical axis line shows zero change.

From 2004 to 2022, global mean ΔDIC_{total} derived from GCC-DIC in the upper 50 m was 1.0 ± 0.23 μmol kg^{-1} yr^{-1}, consistent with previous studies (Sabine et al., 2004; Gruber, Clement, et al., 2019). The rate of DIC_{total} increase attenuated with depth, reaching 0.1 ± 0.13 mol kg^{-1} yr^{-1} near 2000 m (Fig. 1). Over 90% of the DIC_{total} increase in the upper 50 m during the study period (2004–2022) was attributable to ΔDIC_{anth}. This pattern reflects the dominance of anthropogenic CO_2

invasion over biological or carbonate pump processes on (multi-)decadal timescales, consistent with expectations under transient climate forcing (Keppler et al., 2023; Frenger et al., 2024).

The contribution of the BCP to ΔDIC_{total}, ΔDIC_{soft}, did not differ from zero within the uncertainty bounds and remained globally small, with a mean of 0.05 ± 0.09 μmol kg^{-1} yr^{-1} in the upper 50 m (Fig. 1). This negligible contribution was expected, as the BCP primarily redistributes carbon vertically rather than adding new DIC to the system (Passow & Carlson, 2012), so its net impact on globally averaged DIC_{total} remained small on decadal timescales (Martin et al., 1987; Burd et al., 2010; Henson et al., 2011; Boyd et al., 2019). This observation is consistent with recent work emphasizing that the climatic relevance of the BCP arises not from net DIC addition to the ocean's interior but from the sequestration of remineralized DIC_{soft} at depth, isolating it from the surface ocean and atmosphere (Frenger et al., 2024). As such, changes in the vertical distribution of DIC_{soft} may reflect evolving storage patterns rather than changes in its global inventory.

ΔDIC_{carb} did not contribute significantly to global DIC change between 2004 and 2022, as it remained indistinguishable from zero at all depths, and is therefore excluded from further analysis.

Biological carbon pump redistribution

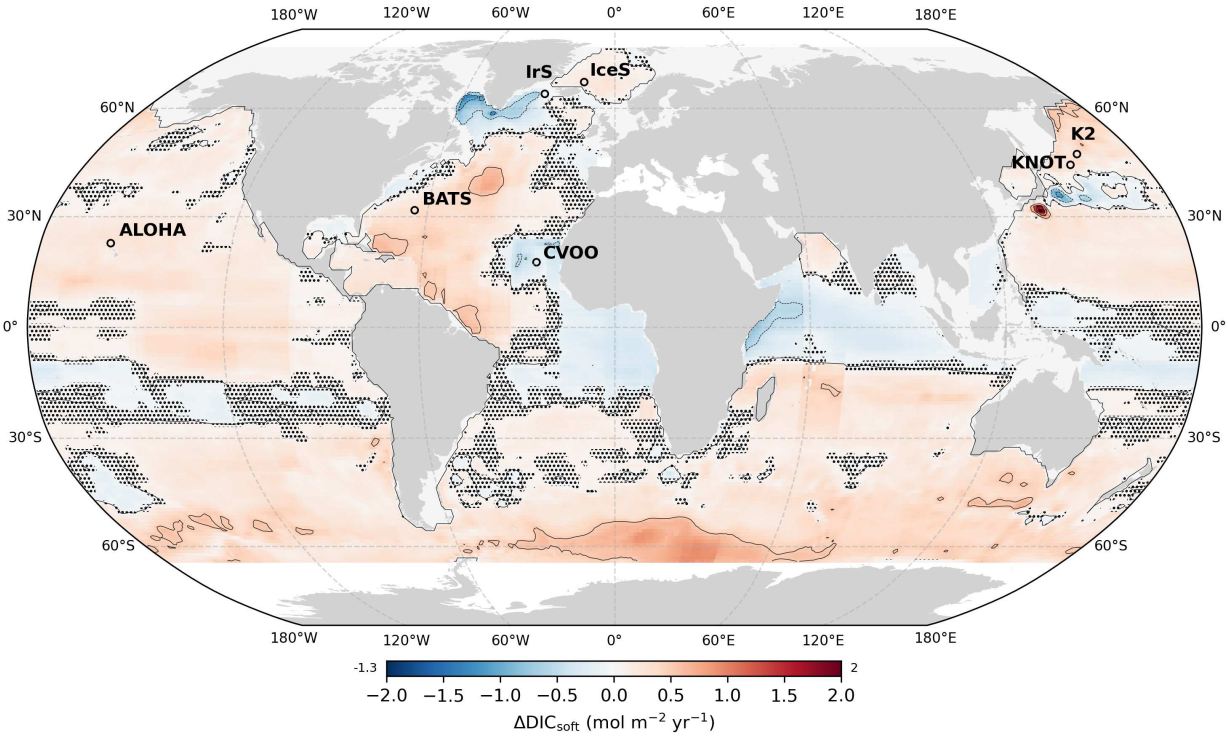

Figure 2. Spatial redistribution of the soft tissue pump's return flux through depth-integrated (i.e., 2.5 to 1975 m) rates of change in DIC_{soft} from 2004 to 2022 for the GCC-DIC product. Units are mol m^{-2} yr^{-1}, calculated by converting local trends in ΔDIC_{soft} (Fig. 1) to volumetric units and integrating from 2.5 to 1975 m depth. Locations of independent ocean time series from the SPOTS compilation (Lange et al., 2024), used for validation, are shown as labelled circles. Comparison with these in situ time series confirms that GCC-DIC aligns with observed variability while also highlighting deviations that may stem from short-term fluctuations in trend emergence (Figs. S7, S8, S9; see Methods; Henson et al., 2016; Lange et al., 2024). Uncertainty in ΔDIC_{soft} is quantified as the standard deviation across a Monte Carlo ensemble (n = 1000) incorporating measurement and stoichiometric uncertainty. Stippling highlights grid cells

where the relative uncertainty exceeds the 90th percentile globally, indicating low signal-to-noise ratios. Contours lines are drawn every 0.5 mol m^{-2} yr^{-1}. Minimum and maximum values are displayed at the ends of the color bar.

Despite no change in ΔDIC_{soft} globally (Fig. 1), our analysis exposes regional shifts in DIC_{soft} storage (Fig. 2). This spatial variability reflects climate-driven shifts in physical, biogeochemical, and ecological processes that are reshaping the efficiency and structure of BCP-driven carbon sequestration (Zhao et al., 2025).

The return flux of the soft tissue pump, when integrated over the upper 2 km, appears to have decreased across the equatorial Atlantic and Indian Oceans, and south subtropical Pacific (Fig. 2). This trend is consistent with the effects of climate-driven ocean warming, which enhances stratification, reduces nutrient supply to the euphotic zone, and ultimately limits net primary production (Laufkötter et al., 2016; Boyd et al., 2019; Wilson et al., 2022; Zhao et al., 2025). Reduced particle export likely limited the transfer of remineralized carbon to depth, as seen in subtropical gyres where declining DIC_{soft} dominates the sequestration signal (Fig. 2). Increased stratification may also have shoaled POC remineralization, thereby increasing the proportion of DIC_{soft} retained at shallower depths and reducing the fraction transferred to long-term storage (Nowicki et al., 2022; Ricour et al., 2023).

Conversely, several regions showed an increase in depth-integrated DIC_{soft} over the upper 2 km. Across most of the Southern Ocean, positive trends in depth-integrated DIC_{soft} correspond to areas where reduced sea-ice extent and enhanced vertical mixing have promoted nutrient supply and larger phytoplankton blooms (Arteaga et al., 2019; Henley et al., 2020; Sallée et al., 2021). These conditions likely favored high POC export efficiency, leading to deeper remineralization and greater accumulation of DIC_{soft} in the mesopelagic. This aligns with positive depth-integrated ΔDIC_{soft} across the Southern Hemisphere's subpolar and subtropical basins, particularly in the Southern Ocean where vertical profiles also reveal deep remineralization and subsurface accumulation (Fig. 4a). In these areas, the BCP's return flux may have increased on interannual to decadal timescales due to climate-driven circulation shifts, including intensified Ekman divergence and strengthened subduction, which influence the vertical redistribution and retention timescales of DIC_{soft} in the ocean interior (Boyd & Trull, 2007; DeVries et al., 2012).

The vertical redistribution of DIC_{soft} is not solely governed indirectly by nutrient-driven changes in export efficiency, but also directly by shifts in ecosystem structure. Warming, acidification, and nutrient limitation have been linked to shifts toward smaller phytoplankton and reduced diatom dominance, leading to slower-sinking particles with shallower remineralization depths (i.e., more DIC_{soft} in the upper mesopelagic; Laufkötter et al., 2016; Kwiatkowski et al., 2020; Barrett et al., 2025). These ecosystem shifts may have resulted in the pronounced decrease in depth-integrated DIC_{soft} observed in the western subtropical Pacific (Fig. 2), regions where enhanced stratification has reduced overall particle export without compensatory increases in nutrient supply from upwelling or vertical entrainment. Although stratification can increase shallow DIC_{soft} accumulation, the net integrated effect is a decrease in long-term carbon storage at depth. These changes not only reduce POC export efficiency but may also shorten the sequestration timescale of the resulting DIC_{soft}.

In contrast, regions typically associated with high nutrient supply and POC export—such as equatorial upwelling zones and coastal upwelling systems adjacent to eastern boundary currents—

show mixed signals in depth-integrated ΔDIC_{soft} (Fig. 2). While some areas (e.g. eastern tropical Pacific) exhibited neutral or weakly positive ΔDIC_{soft} when integrated from 2.5 to 1975 m, others (e.g. eastern tropical Atlantic near CVOO) showed negative values despite persistent upwelling (Koseki et al., 2024). These discrepancies likely arose from decoupling between surface POC export and deeper DIC_{soft} sequestration: enhanced POC export at the surface can coincide with shallower remineralization of organic matter under warming and deoxygenation, reducing the effectiveness of deep DIC_{soft} sequestration despite sustained surface productivity (Marsay et al., 2015; Weber et al., 2016; Henson et al., 2019; Frenger et al., 2024). While warming accelerates microbial respiration, moderate deoxygenation may shift remineralization into shallower, suboxic zones, where anaerobic microbial processes continue the degradation of POC. However, in fully anoxic or euxinic waters, remineralization may slow, potentially enhancing deep transfer by limiting zooplankton and aerobic microbial activity (Cavan et al., 2017; Oschlies et al., 2018).

The subpolar gyre of the North Atlantic displays a dipolar pattern, with positive ΔDIC_{soft} in the western subpolar and Arctic outflow regions, but negative values near deep-water formation zones such as the Labrador and Irminger Seas. These opposing trends suggest that reduced ventilation and weakened overturning circulation (Yashayaev & Loder, 2016; Caesar et al., 2018) may have suppressed the delivery of DIC_{soft} to the interior in some regions while enhancing subsurface accumulation elsewhere. In surface layers, anthropogenic CO_2 uptake can also mask biologically-driven changes in the DIC_{soft} inventory, particularly in regions with strong air–sea CO_2 fluxes (Gruber et al., 2023; Asselot et al., 2024; Nowicki et al., 2024). As such, the observed patterns in ΔDIC_{soft} reflect net biological effects superimposed on background anthropogenic signals, especially in high-latitude and high-CO_2-flux zones (Gruber, Landschützer, et al., 2019; Nowicki et al., 2024).

Overall, the spatial variability in ΔDIC_{soft} did not signal a globally uniform weakening or strengthening of the BCP, but rather a redistribution arising from regional changes in POC export efficiency and the subsequent vertical transport and storage of respired DIC_{soft} (Frenger et al., 2024). Regional processes driven by climate-linked changes in stratification, nutrient pathways, and ecosystem dynamics appear to offset each other at the global scale (Friedlingstein et al., 2023). Yet this apparent compensation may be decadal and non-stationary. As regional imbalances accumulate, they may eventually destabilize the BCP's global sequestration efficiency, particularly if key thresholds in stratification or deoxygenation are crossed. Whether this compensation can persist under accelerating climate change remains an open question.

Dynamic sequestration horizon

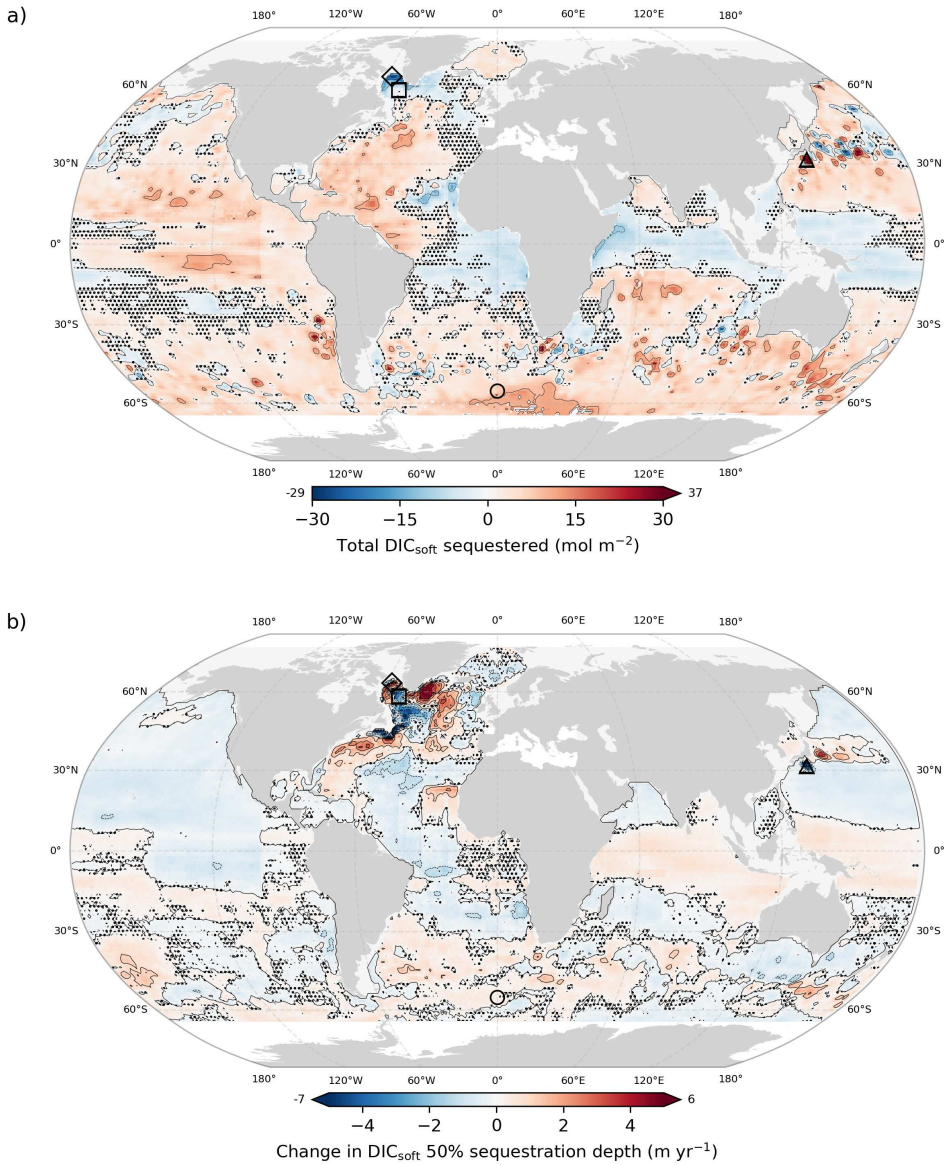

Figure 3. (a) Net ΔDIC_{soft} (mol m^{-2}) sequestered below the maximum climatological MLD and down to 1975 m, and (b) change in DIC_{soft} 50% sequestration depth (m yr^{-1}), both from 2004 to 2022 based on the GCC-DIC dataset. Values in (a) reflect the time-integrated accumulation of biologically sequestered carbon below the maximum mixed layer depth (MLD) extending the depth-integrated annual rates shown in Figure 2. Positive trends in (b) indicate a deepening of carbon storage; negative trends indicate shoaling. Uncertainties were quantified as the standard deviation across a Monte Carlo ensemble (n = 1000) incorporating measurement and stoichiometric uncertainties. Stippling highlights grid cells where the relative uncertainty exceeds the 90th percentile globally, indicating low signal-to-noise ratios. In (a), this uncertainty reflects variability in sequestration estimates while in (b), it indicates greater sensitivity where changes in sequestration depth are small or highly variable. Contours lines are drawn every 10 mol m^{-2} for (a) and every 1 m yr^{-1} for (b). Minimum and maximum values for each panel are displayed at the ends of the respective colorbars. Locations corresponding to the four quadrant scenarios illustrated in Figure 4 are also marked: (a) increasing carbon storage and deepening remineralization (circle, 55°S 0°E); (b) reduced storage and shoaling remineralization (square, 58°N 51°W); (c) increased carbon at depth but shallower mean remineralization (triangle, 31.5°N 136.5°E); and (d) declining storage but deeper remineralization (diamond, 63.5°N 57.5°W).

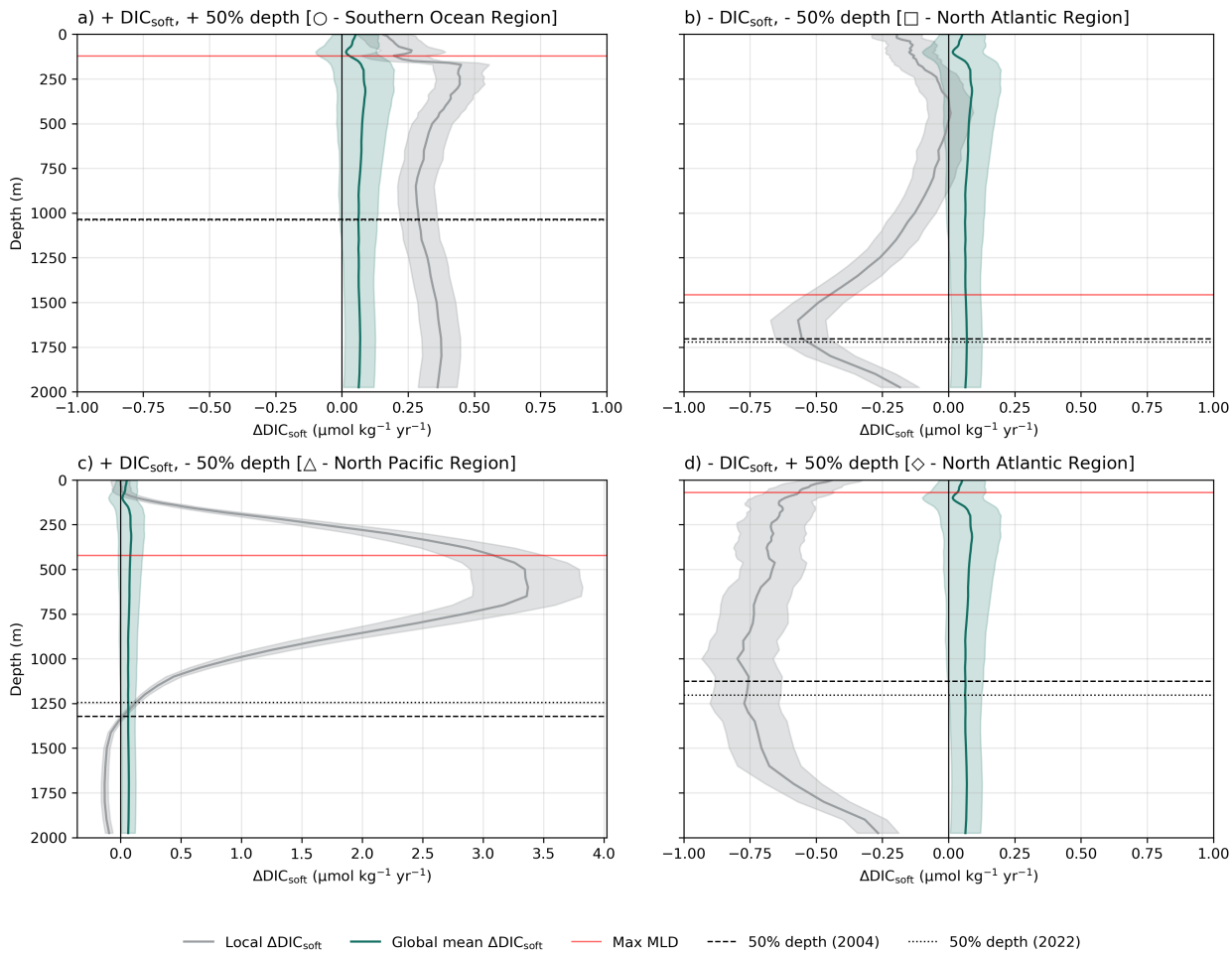

Figure 4. Local rates of change in DIC_{soft} as a function of depth (m) within the upper 1975 m for the GCC-DIC dataset at four representative locations, as shown in Figure 2. Global mean rate of change in DIC_{soft} as seen in Figure 1 is shown in green. The horizontal red line indicates the site-specific maximum climatological mixed layer depth (MLD_{max}) from Holte et al. (2017), while the dashed and dotted lines show the yearly mean 50% sequestration depths of DIC_{nat} for 2004 and 2022, respectively. Panels illustrate four scenarios following Figure 3: (a) increasing carbon storage and deepening remineralization (circle, 55°S 0°E); (b) reduced storage and shoaling remineralization (square, 58°N 51°W); (c) increased carbon at depth but shallower mean remineralization (triangle, 31.5°N 136.5°E); and (d) declining storage but deeper remineralization (diamond, 63.5°N 57.5°W). Note the different x-axis range for c). These locations were selected to illustrate extreme cases of each scenario, acknowledging that the clarity of the signal depends on the magnitude of change in either DIC_{soft} (Fig. 3a) or in the 50% sequestration depth (Fig. 3b). Despite this heterogeneity, the pairwise Wasserstein distances between residual profiles (computed as the difference between the maximum and minimum annual DIC_{soft} profiles at each grid cell; see Methods and Supplementary Information) remained low within each scenario (mean WD: 2.8–3.9 μmol m kg^{-1}; Table S3), indicating coherent vertical patterns across the global ocean.

The BCP's reorganization extends beyond surface POC export, altering both the depth and duration of respired DIC_{soft} retention in the ocean interior. (DeVries et al., 2012; Boyd et al., 2019; Ricour et al., 2023). The depth at which biologically sequestered DIC_{soft} accumulates plays a key role in regulating atmospheric CO_2, with deeper storage associated with longer isolation times (DeVries et al., 2012). This vertical dimension is evident in the total amount of DIC_{soft} stored below the winter mixed layer (Fig. 3a; Fig. 4) and in the shifting depth at which that carbon is retained (Fig. 3b; Fig. 4), both of which show distinct regional trends over the 2004–2022 period.

Simultaneous changes in DIC_{soft} inventory and sequestration depth indicate a coordinated reorganization of the BCP, reflecting shifts in both the magnitude and vertical structure of carbon storage (Fig. 3; Fig. 4). Regions with increases in both, like in the Southern Ocean and parts of the subtropical South Atlantic and Indian gyres, point to strengthened export of POC and deeper remineralization to DIC_{soft}, suggesting enhanced long-term sequestration potential (Fig. 3; Fig. 4a). Conversely, regions where both are negative, including parts of the western subtropical North Pacific, reflect shoaling of DIC_{soft} return pathways and possible decreases in the sequestration efficiency of this respired carbon (Fig. 4b; Wilson et al., 2022; Siegel et al., 2023). However, in several regions, the relationship between DIC_{soft} accumulation and sequestration depth is decoupled, reflecting divergent trajectories in vertical carbon retention (Fig. 4c-d). While the depth-integrated DIC_{soft} signal offers a direct measure of long-term carbon storage, changes in sequestration depth provides insight into future trajectories. A shoaling trend could imply a gradual re-exposure of previously isolated DIC_{soft} to the surface mixed layer, while deepening may signal enhanced isolation. The emergence of these divergent patterns, where changes in DIC_{soft} inventory and sequestration depth do not align, suggests that vertical sequestration structure may be increasingly climate-sensitive, shaped by warming, stratification, oxygenation, and ecosystem shifts (Boyd et al., 2016; DeVries, 2018; Bindoff et al., 2019; Boyd et al., 2019; Li et al., 2020; Wilson et al., 2022; Zhao et al., 2025). While the exact mechanisms remain unresolved, the spatial coherence of these trends is consistent with a potential reorganization of the biological carbon pump, which could represent an emerging feedback in the Earth's climate system.

Sequestration of biologically stored carbon (both as POC and respired DIC_{soft}) occurs across a broad range of depths, rather than being limited to the deep ocean below 2000 m. This has been highlighted by recent work showing that regional circulation and remineralization patterns govern the depth at which biologically derived carbon is retained (Ricour et al., 2023). Variability in sequestration depth of DIC_{soft} is emerging as a determinant driver of climate sensitivity, one that can alter carbon retention timescales and accumulate long-term impacts, even in the absence of major shifts in the magnitude of surface export of POC (Ricour et al., 2023). This vertical decoupling of export, remineralization, and depth of storage has the potential to destabilize regional carbon retention patterns and weaken the BCP's role as a long-term carbon sink (Wilson et al., 2022; Siegel et al., 2023). Model intercomparison studies show that this uncertainty grows with depth, with CMIP6 projections of POC flux at 1000 m ranging from a 4% increase to a 55% decline by 2100, highlighting major differences in how transfer efficiency and deep-ocean sequestration are parameterized (Walker & Palevsky, 2025).

However, current Earth system models do not fully account for this climate-sensitive variability in carbon sequestration (Henson et al., 2022; Wilson et al., 2022). Most rely on fixed remineralization profiles and assume constant sequestration depths, despite mounting evidence that both are responsive to climate-driven changes in ocean physics and ecosystem structure

(Ricour et al., 2023). Additional stressors, such as ocean acidification, are already altering carbonate mineral production and the chemical buffering capacity of seawater, introducing further biogeochemical feedbacks (Barrett et al., 2025). Failing to incorporate these mechanisms may bias projections of future ocean carbon uptake and its capacity to moderate anthropogenic emissions (Henson et al., 2022; Gruber et al., 2023; Koeve et al., 2024; Barrett et al., 2025).

As model projections diverge on whether POC export will strengthen, weaken, or redistribute under climate change (Henson et al., 2022), observed changes in the depth and distribution of DIC_{soft} provide a critical constraint on the BCP. The emergence of coherent trends, both positive and negative, may represent the first detectable signs of BCP destabilization (Fig. 2; Fig. 3; Fig. 4). Although a complete mechanistic understanding is still emerging, these patterns may serve as early warning signals of how climate-driven changes in the upper ocean are beginning to reshape deep ocean carbon storage, even before global net export fluxes shift appreciably. (Gruber et al., 2023; Koeve et al., 2024).

Together, these findings point to a shift in how we should assess the stability of the BCP. While globally averaged ΔDIC_{soft} has remained virtually zero in recent decades, this apparent consistency masks regional and vertical imbalances in where and how carbon is sequestered. Such structural changes, particularly in sequestration depth and thus retention time, may precede a change in efficiency of the marine carbon sink. Export flux alone is not a sufficient indicator of BCP efficiency. Instead, the depth at which respired carbon is stored, how long it remains sequestered, and its eventual fate should all be considered to evaluate the BCP's evolving role in climate regulation. As climate change intensifies, monitoring the relationship between export and long-term storage of marine DIC_{soft} will be critical for projecting how future feedbacks between ocean biology, circulation and the atmosphere will affect atmospheric CO_2 levels and the global carbon cycle.

Methods

GOBAI-O_2 v2.1 database

GOBAI-O_2, short for Gridded Ocean Biogeochemistry from Artificial Intelligence – Oxygen (Sharp et al., 2023), is a data product that provides three-dimensional monthly fields of dissolved oxygen. Covering 86% of the global ocean area on a 1° × 1° latitude-longitude grid, GOBAI-O_2 v2.1 spans from 2004 to 2022 and extends from the ocean surface down to a depth of 2 km across 58 levels. It was constructed using machine learning algorithms, specifically random forest regressions and feed-forward neural networks, trained on oxygen concentration ([O_2]) data from discrete shipboard measurements and autonomous sensors on BGC-Argo floats (Sharp et al., 2023). The application of these algorithms to three-dimensional monthly gridded fields of temperature and salinity was validated using both real observations and simulated data from Earth system model outputs. The temperature and salinity input fields were derived from the Argo climatology of Roemmich and Gilson (2009). The total combined uncertainty is 7.6 µmol kg^{-1} on average globally, reaching 11.2 µmol kg^{-1} at 150 dbar, which aligns with a root mean square deviation (RMSD) of 8.8 µmol kg^{-1}, independently validated by withholding data from the model training set.

Reconstruction of DIC time series using CANYON-B and CONTENT algorithms

The CANYON-B (CArbonate system and Nutrients concentration from hYdrological properties and Oxygen using a Neural-network) and CONTENT (CONsisTency EstimatioN and amounT) algorithms were developed for estimating dissolved inorganic carbon (DIC), total alkalinity (TA), pH, and partial pressure of CO_2 (pCO_2), as well as nutrients (Sauzède et al., 2017; Bittig et al., 2018) . CANYON-B is a Bayesian neural network that estimates nutrients and carbonate system variables from oxygen concentration, temperature, and salinity, based on biogeochemical relationships identified in the GLODAPv2 bottle dataset (Sauzède et al., 2017). In contrast, CONTENT refines and integrates the four carbonate system variables, ensuring internal consistency with established carbonate chemistry (Bittig et al., 2018).

Both algorithms include uncertainty estimates, which were formulated by incorporating local environmental conditions. They were validated against independent GO-SHIP bottle data and in situ sensor observations, including biogeochemical floats and shipboard sensors, and have demonstrated favorable performance relative to other estimation approaches. The CONTENT algorithm estimates the uncertainty of DIC with values ranging from 7.7 µmol kg^{-1} at the 10th percentile to 11.8 µmol kg^{-1} at the 90th percentile, with a median (50th percentile) uncertainty of 9.1 µmol kg^{-1} (Bittig et al., 2018).

The GOBAI-O_2 dataset (i.e. T, S and O_2; v.2.1; see previous section) was integrated into the CANYON-B and CONTENT algorithms to derive key CO_2 system parameters. Among these, DIC and TA were estimated on a 1° × 1° grid from 2004 to 2022, covering 58 depth levels from 2.5 m to 1975 m (Figs. S1–S2 in Supplementary Information).

Throughout this study, the term GCC-DIC (GOBAI-O_2 CANYON-B CONTENT-DIC) refers to DIC estimates derived from the application of the CANYON-B and CONTENT algorithms to the GOBAI-O_2 dataset (see Figs. S1–S2 in the Supplementary Information) and is used interchangeably with "reconstruction."

Independent ocean CO_2 time series

To validate the changes observed in the GCC-DIC product, we analyzed independent ocean CO_2 time series data at selected ocean time series stations from the Synthesis Product for Ocean Time Series (SPOTS; Table S1, Fig. S7 in Supplementary Information) product Lange et al. (2024). Figure S7 illustrates the selected profiles through time at each site, based on predefined neutral density boundaries. This selection ensures a consistent water mass is analyzed across years, maximizing temporal coverage while retaining sufficient data density for robust trend detection.

Subsequently, each time series was analyzed to identify either a positive or negative rate of change across the study period (2004–2022) in DIC and its components, in relation to its position within the global analysis conducted using the synthetic product. The key objective was to evaluate whether the long-term trends reconstructed by GCC-DIC at selected sites are consistent with independent in situ observations. Results from the in-situ time series validating GCC-DIC are presented in Figures S8, S9 and S10, as well as Table S2 in the Supplementary Information.

The same analytical approach, detailed in the subsequent Methods sections, was applied to both the GCC-DIC product and the SPOTS in situ time series, unless stated otherwise.

Decomposition of DIC components

The changes in DIC within the ocean are primarily governed by three processes: the absorption of anthropogenic CO_2 from the atmosphere (DIC_{anth}), the action of the BCP responsible for natural carbon cycling (DIC_{soft}), and the carbonate pump, which is linked to the formation and dissolution of calcium carbonate (Volk & Hoffert, 1985; Gruber et al., 1996). These processes contribute to DIC as follows:

$$\mathrm{DIC} = \mathrm{DIC_{anth}} + \mathrm{DIC_{soft}} + \mathrm{DIC_{carb}} \quad (1).$$

The uptake of anthropogenic CO_2 is often referred to as the solubility pump. Assuming no significant trends in the air-sea CO_2 disequilibrium over the long term, the anthropogenic (DIC_{anth}) is effectively equivalent to the solubility-derived DIC (DIC_{sol}), ignoring short-term and regional disequilibrium variations. The rationale for considering $DIC_{diseq} = 0$ is supported by the minimal impact of long-term disequilibrium trends on the global carbon uptake over the periods studied (Jones et al., 2014; Nowicki et al., 2024).

$$\mathrm{DIC_{anth}} = \mathrm{DIC_{sol}} - \mathrm{DIC_{diseq}} \approx \mathrm{DIC_{sol}} \quad (2),$$

Biological activity transforms dissolved inorganic nutrients into particulate organic matter through the processes of photosynthesis and remineralization and is known as the soft tissue pump(Redfield, 1958; Redfield, 1963; Volk & Hoffert, 1985). This process drives the downward export of particulate organic carbon (POC) from the surface ocean, followed by its microbial remineralization into DIC_{soft} at depth, and the subsequent redistribution of respired DIC_{soft} by ocean circulation (Dugdale & Goering, 1967; Boyd et al., 2019). The efficiency and depth of remineralization regulate the extent of DIC_{soft} sequestration and its climate impact over relevant timescales (Figure S3 in Supplementary Information).

This transformation follows specific stoichiometric proportions, quantified by the Redfield ratio, which describes the relationship between the elemental composition of marine organic matter and the nutrients consumed (Redfield, 1958). These materials are transported to deeper waters by gravitational settling and biological transport, where they decompose back to inorganic forms, thereby consuming oxygen and increasing apparent oxygen utilization (AOU). AOU represents the difference between the oxygen concentration at saturation (the theoretical maximum in equilibrium with the atmosphere) and the actual oxygen concentration in seawater, with higher values indicating more oxygen consumption due to remineralization (Garcia & Gordon, 1992). The impact of remineralization on DIC, termed DIC_{soft}, can be quantified using the Redfield ratio as:

$$\mathrm{DIC_{nat}} = -\mathrm{R_{C/O_2}} \cdot \mathrm{AOU} \quad (3).$$

In this study, we used the ratio from (Anderson & Sarmiento, 1994) as follows:

$$\begin{matrix} \mathrm{P:N:C:O_2} \\ 1:16:117:-170 \end{matrix} \quad (4).$$

Thus, $\mathrm{R_{C/O_2}}$ can be assumed to be a constant value of -0.688 ± 0.092 (Anderson & Sarmiento, 1994).

The formation and dissolution of calcium carbonate, described as the carbonate pump, are associated with changes in TA. The carbonate-related DIC_{carb} is affected by the ratio of nitrogen to oxygen during these processes, represented as:

$$\mathrm{DIC_{carb}} = 0.5 \cdot \left(\mathrm{TA} - \mathrm{R_{N/O_2}} \cdot \mathrm{AOU}\right) \quad (5),$$

where $\mathrm{R_{N/O_2}}$ is -0.0941 ± 0.0081 (Anderson & Sarmiento, 1994), indicating how carbonate processes alter DIC by a two-fold increase in TA.

While the Redfield ratio is known to exhibit regional and temporal variability, its use as a constant here provides a first-order global estimate of biologically driven DIC changes, consistent with prior large-scale studies (Anderson & Sarmiento, 1994; Gruber et al., 1996). Similarly, the use of AOU as a proxy for remineralization-driven DIC changes offers a widely accepted and practical approach for estimating DIC_{soft} at large spatial scales. Nevertheless, AOU-based methods assume that surface waters are in equilibrium with the atmosphere at the time of subduction, which may not always hold true—particularly in regions such as the North Atlantic, where rapid subduction can preserve disequilibrium signals (Ito et al., 2004; Sulpis et al., 2023). While such deviations are unlikely to dominate global-scale estimates, they may introduce regional biases and should be considered when interpreting patterns of biological carbon cycling.

Neutral density and pressure dimensions

In theory, neutral density surfaces represent oceanic mixing processes that occur along isopycnal surfaces. However, adopting the neutral density dimension means forgoing a gridded product, which facilitates practical analysis of changes in DIC components across the global ocean. Thus, in our study, we determined whether vertical water mass movements (heave), averaged over the

studied period, could be adequately analyzed within the pressure dimension, or if using neutral density was necessary.

To explore the differences between pressure and neutral density as analytical dimensions, pixels from various ocean basins were isolated and analyzed in both pressure and neutral density spaces (see Figure S4 of the Supplementary Information).

We then assessed the variations in pressure across different ocean basins by quantifying how the relationship between pressure and neutral density fluctuated over time. For each predefined ocean basin, we calculated the ratio of pressure (P) to neutral density (γ) for all pressure levels in the 4D synthetic product:

$$\mathrm{Ratio}_{P/\gamma} = \frac{P}{\gamma} \quad (6).$$

Using the ratio of pressure to neutral density provides normalization across basins, enabling consistent comparison of regions with different absolute values of pressure and density. Additionally, it simplifies dimensional consistency and highlights subtle fluctuations over time, making it more sensitive to small-scale variability. By comparing these ratios to their mean values over the entire time period (2004-2022), we were able to determine residuals, which represent deviations from the mean relationship between pressure and neutral density:

$$\mathrm{Residuals} = \frac{P}{\gamma} - \left(\frac{P}{\gamma}\right)_{\mathrm{mean}} \quad (7).$$

This part of the analysis revealed no significant long-term trends in the pressure/γ (gamma) ratio, indicating that pressure has remained stable with respect to neutral density over the study period. This conclusion is supported by linear regressions on the time series of mean residuals across all pressure levels, which showed no significant trends in any ocean basin ($p > 0.05$; Fig. S4 in the Supplementary Information, see Methods for details).

To make these deviations interpretable in terms of pressure changes, we converted the residuals back into pressure variations:

$$\Delta P = \mathrm{Residuals} \times \frac{P}{\gamma} \quad (8).$$

This allowed us to quantify the minimum and maximum pressure changes at each pressure level for every basin. These extreme pressure variations provide insight into the range of variability in the relationship between pressure and neutral density across different ocean basins and time periods.

The largest deviation (ΔP) observed across the study period (2004 – 2022) was approximately 6 dbar, occurring in the North Atlantic (Figure S6 of the Supplementary Information). This corresponds to ~6m, a relatively small fluctuation in the context of oceanic processes. Given the absence of consistent trends in $\mathrm{Ratio}_{P/\gamma}$ and considering that the analysis integrates over the entire pressure column, these variations appear insignificant. Therefore, the pressure dimension remains a reliable and practical choice for the continuation of this analysis (Fig. 3, Fig. S9 of the Supplementary Information). For simplicity, we use pressure and depth interchangeably, as the

difference remains small (<~2%) down to 2000 m and does not affect the interpretation of our results (Saunders & Fofonoff, 1976; Wunsch & Webb, 1979).

Rates of change in DIC components

To quantify changes in each component of DIC, we employed an ordinary least-squares linear regression on the gridded 4D product GCC-DIC. We first computed annual global mean vertical profiles by averaging across all latitude and longitude grid points. Linear trends were then estimated at each depth level based on these yearly global averages (Fig. 1).

Then, change was analyzed at a finer resolution for each pixel within the gridded product, allowing for spatially resolved trend estimates. Linear regression was applied to each grid cell's time series to compute annual rates of change (μmol kg^{-1} yr^{-1}) for DIC and its components. To estimate depth-integrated changes, these trends were first converted to mol m^{-3} yr^{-1} using in situ density. Each trend value was then scaled by the thickness of the layer it represents, defined as the pressure difference between consecutive levels (i.e., between depth level i and i+1). The resulting values were summed across all levels to obtain the total change over the water column (mol m^{-2} yr^{-1}), effectively representing a local DIC budget. Finally, the depth-weighted mean DIC trend was computed by dividing the total by the full water column thickness (Fig. 2). This approach provides a depth-integrated rate of change in units of mol m^{-2} yr^{-1}.

Independent ocean time series were not uniformly gridded like GCC-DIC, thus interpolation was necessary to align them correctly. All variables were vertically interpolated along the pressure dimension using piecewise cubic Hermite interpolating polynomials (Fritsch & Carlson, 1980). This method uses monotonic cubic splines to precisely calculate the values at new points, facilitating depth-specific analysis. Then, an ordinary least squares linear regression was applied to each pressure level to determine the rate of change in each variable over time along the water column (Fig. 3, Fig. S8 and S9 of the Supplementary Information).

Calculation of DIC_{soft} fluxes below the MLD

The mixed layer depth (MLD) was derived from the Argo-based climatology compiled by Holte et al. (2017). This method uses a combination of profile shape analysis, threshold, and gradient criteria to estimate MLD from individual Argo profiles. The climatology includes over 2.6 million Argo profiles collected between 2000 and 2022 and provides monthly MLD statistics on a 1° × 1° grid. For this study, we used the global maximum MLD, calculated as the average of the three deepest MLDs within each monthly bin, to define the lower boundary of the surface layer for carbon storage analysis (Fig. S11 in the Supplementary Information).

To align the MLD product with the DIC product, the maximum climatological MLD was extracted for each grid cell and interpolated onto the DIC product's latitude and longitude grid using bilinear interpolation. This ensures that MLD values are spatially consistent with the DIC measurements while preserving the original MLD distribution.

Following the determination of the MLD, DIC_{soft} concentrations were considered for the water column extending from the MLD to the bottom (i.e., 2000 m). DIC_{soft} was initially presented in

μmol kg^{-1} and was converted to mol m^{-3} using in situ density measurements, facilitating an accurate representation of DIC quantities per volume of seawater.

To integrate DIC_{soft} vertically through the water column, the thickness of each discrete layer (defined by the product's pressure increments) was calculated. The total amount of DIC_{soft} sequestered below the MLD was then quantified by summing the products of DIC concentrations (in mol m^{-3}) and the corresponding layer thicknesses across the entire depth range below the MLD. This integration yielded an estimate of the total moles of DIC_{soft} per square meter of seabed area (mol m^{-2}), providing a comprehensive measure of DIC storage within the sub-MLD water column.

To assess changes in DIC_{soft} storage over time, the differences in integrated DIC_{soft} from one time point to the next were calculated (i.e., using the monthly resolution of GCC-DIC). Summing of these differences provided a cumulative measure of net new DIC_{soft} sequestration (Fig. 2b).

Change in 50% DIC_{soft} sequestration depth

To assess temporal variations in the depth of DIC_{soft} sequestration below the MLD, we computed the cumulative integrated dissolved inorganic carbon (DIC) concentrations below the MLD at each time-series site. As for the calculation of DIC_{soft} fluxes, the climatological MLD was extracted for each site's latitude and longitude and interpolated onto the DIC product's spatial grid using nearest-neighbor interpolation.

To calculate the sequestration depth of DIC_{soft}, we first determined the total integrated DIC_{soft} below the MLD at each site by multiplying DIC_{soft} concentrations by the seawater density at each depth level and summing over all levels. The 50% sequestration depth was then identified as the shallowest depth at which the cumulative integrated DIC_{soft} exceeded 50% of the total integrated DIC_{soft} below the MLD. This depth represents the median sequestration depth of DIC_{soft} over time and serves as an indicator of changes in vertical carbon storage.

DIC_{soft} sequestration depth time series were smoothed using locally weighted scatterplot smoothing (LOESS; smoothing fraction = 0.5) to reduce high-frequency variability (Cleveland, 1979; Cleveland & Devlin, 1988). LOESS smoothing was applied specifically to the DIC_{soft} sequestration depth because this variable represents a derived percentile-based metric (i.e., the 50% depth of integrated DIC_{soft}) that is highly sensitive to short-term fluctuations, especially in shallow depth levels with steep gradients. Unlike concentration-based variables, which benefit from a high signal-to-noise ratio due to volume integration, the 50% sequestration depth is a single-point threshold that can shift significantly with small changes in the vertical profile. Moreover, sequestration depth is not consistently defined at all time steps (e.g., when integrated DIC_{soft} is very low, the 50% threshold may fall near a noisy transition zone), which increases the need for a robust smoothing method like LOESS to isolate long-term.

Both GCC-DIC and the SPOT in-situ time series required a method to resolve seasonal and interannual variability. Interannual fluctuations are expected in long-term records, but uneven sampling complicates deseasonalization. LOESS adaptively smooths data by weighting nearby observations, capturing broad trends, and filtering short-term noise. Temporal trends were quantified using ordinary least squares (OLS) linear regression on the smoothed time series, from which the slope (m yr^{-1}) and p-value were extracted. Differences in sequestration depth between

the first (Q1) and last (Q4) quartiles of the observation period were evaluated using a two-sample Welch's t-test (Welch, 1947), with changes considered significant at $p < 0.05$.

Uncertainty estimates for the temporal trends were calculated by propagating the standard errors from the linear regression. Standard errors for mean sequestration depths in Q1 and Q4 were computed as the standard deviation divided by the square root of the number of observations. The total uncertainty in sequestration depth change was propagated from these standard errors using standard error propagation methods.

Error Propagation

To account for uncertainties in DIC component trends, we implemented a Monte Carlo simulation with 1,000 iterations. In each iteration, random perturbations were introduced to DIC, alkalinity, and apparent oxygen utilization (AOU) based on their respective measurement uncertainties. DIC and TA uncertainties were derived from the CANYON-B algorithm, and AOU uncertainties included both the measurement errors in dissolved oxygen and those associated with the CONTENT-derived oxygen saturation (Sauzède et al., 2017; Bittig et al., 2018). These uncertainties were assumed to follow Gaussian distributions with standard deviations matched to the reported algorithmic uncertainties at each data point.

In addition, uncertainties in the soft-tissue and carbonate pump scaling factors were incorporated by perturbing their values using normal distributions derived from reported errors (Anderson & Sarmiento, 1994). For the soft-tissue pump, variability in the respiratory quotient ($C:O_2$) was explicitly modeled by drawing values from a normal distribution with a mean of -0.688 and a standard deviation of 0.092. Similarly, for the carbonate pump, the $N:O_2$ ratio (used in estimating the carbonate-driven DIC component) was sampled from a distribution centered on -0.0941 with a standard deviation of 0.0081.

For each perturbed product, a linear regression was applied at both the global (Fig. 1) and pixel levels (Fig. 2 and 3) to estimate trends in DIC and its components. At the pixel level, perturbed trends were converted to mol/m³ using in-situ density and depth-integrated by scaling them with layer thickness. The Monte Carlo ensemble provided a distribution of possible DIC trends, from which the final estimate was taken as the ensemble mean, while uncertainty was quantified as the standard deviation across all iterations. For global trends, area-weighted averaging was applied across latitude and longitude before computing the final uncertainty estimate. This approach ensures robust error propagation, capturing both measurement uncertainties and variability in scaling relationships.

To estimate uncertainty in the change and sequestration of soft-tissue-driven DIC (DIC_{soft}) below the MLD (Fig. 2, 3 and 4) a separate Monte Carlo approach was implemented. In each iteration, perturbed AOU values were used to estimate DIC_{soft} using a randomly sampled soft-tissue pump scaling factor. The sequestration estimate was constrained to depths below the maximum climatological MLD, interpolated onto the DIC product for consistency. DIC_{soft} values were converted to mol/m³ using in-situ density and integrated over depth using layer thickness derived from pressure differences. The resulting depth-integrated sequestration rates were computed at each time step, with uncertainties propagated iteratively using Welford's method (Welford, 1962;

Knuth, 1969). Specifically, for each new iteration x_n, the updated mean μ_n and variance σ_n^2 were computed recursively as:

$$\mu_n = \mu_{n-1} + \frac{x_n - \mu_{n-1}}{n} \quad (9),$$

$$\sigma_n^2 = \sigma_{n-1}^2 + \frac{(x_n - \mu_{n-1})(x_n - \mu_n)}{n} \quad (10).$$

This method provides an efficient way to update statistical estimates without storing all previous values, ensuring accurate uncertainty quantification over the Monte Carlo iterations while remaining computationally inexpensive.

To assess long-term sequestration trends, year-to-year differences in depth-integrated DIC_{soft} sequestration were computed, and cumulative sequestration was estimated via a running sum over time. Uncertainty in the cumulative sequestration was derived by propagating standard deviations across time steps. The final sequestration estimates and associated uncertainties provide a robust quantification of the storage of biologically driven DIC below the MLD.

Vertical profile classification and analysis by quadrant scenario

To explore the vertical structure of biologically driven carbon storage changes, we identified four types of pixels based on their classification in Figure 3a and Figure 3b. Figure 3a shows the net change in DIC_{soft} sequestration below the maximum climatological mixed layer depth (MLD), while Figure 3b shows the trend in the 50% sequestration depth of DIC_{soft}. Combining the sign of the change from both panels, we categorized each grid cell into one of four scenarios: (1) increased DIC_{soft} sequestration and deeper sequestration depth; (2) decreased DIC_{soft} sequestration and shallower sequestration depth; (3) increased DIC_{soft} sequestration but shoaling sequestration depth; and (4) decreased DIC_{soft} sequestration but deepening sequestration depth.

For each scenario, we analyzed changes in vertical structure by calculating residual profiles of DIC_{soft}. These were defined at each pixel as the difference between the DIC_{soft} profiles in the mean year of maximum and the mean year of minimum using the full water column (2.5–1975 m). This allowed us to isolate the most pronounced temporal changes in carbon storage structure, rather than relying on a linear trend.

To assess the spatial coherence of these vertical changes within each scenario, we calculated pairwise Wasserstein distances between all residual profiles in that scenario. The Wasserstein distance quantifies how much DIC_{soft} would need to be vertically redistributed to transform one profile into another, providing a physically intuitive measure of dissimilarity. Because DIC_{soft} is expressed in units of $\mu mol\ kg^{-1}$ and is distributed over the water column (in m), the resulting distance has units of $\mu mol\ m\ kg^{-1}$. A low mean distance implies a consistent pattern of change across pixels, while a higher value indicates greater variability in vertical structure.

Because some scenarios contained thousands of valid grid cells, we also repeated the analysis on a random 20% subsample of residuals within each scenario. Results from this reduced sample were

highly consistent with the full-sample values, confirming that the observed coherence is robust and not an artifact of large sample size (Table S4 in Supplementary Information).

To illustrate the four conceptual scenarios defined by Figure 3a and 3b, we isolated one extreme case per scenario (i.e., the highest product of ΔDIC_{soft} and sequestration depth trend) and visualized its residual profile in Figure 4.

Data availability

All data and analysis scripts can be accessed at https://doi.org/10.5281/zenodo.15790561. The repository includes the raw data and scripts used to generate the results presented in the manuscript to ensure full reproducibility of results.

Author contributions

HC, LD, MPH, OS, and RS conceptualized the project. LD curated the data. GJR, HC, LD, MPH, OS, PWB, and RS performed the investigation. LD conceptualized the methodology, used the necessary software, visualized the data, and prepared the original draft of the paper. GJR, HC, LD, MPH, OS, PWB, and RS reviewed and edited the paper.

Competing interests

The contact author has declared that neither they nor their co-authors have any competing interests.

Acknowledgements

We thank Jon Sharp for developing the GOBAI-O_2 dataset, which was central to this study. In addition to Jon, we are also grateful to Jon-Andrea Fassbender and Stevie Walker for their valuable insights and feedback during the late stages of this work. Special thanks to Marine Fourrier for her assistance with the MATLAB implementation of the CANYON-B and CONTENT algorithms on the GOBAI-O_2 dataset.

References

Anderson, L. A., & Sarmiento, J. L. (1994). Redfield ratios of remineralization determined by nutrient data analysis. *Global Biogeochemical Cycles*, *8*(1), 65-80. https://doi.org/10.1029/93gb03318

Arteaga, L. A., Pahlow, M., Bushinsky, S. M., & Sarmiento, J. L. (2019). Nutrient controls on export production in the Southern Ocean. *Global Biogeochemical Cycles*, *33*(8), 942-956.

Asselot, R., Carracedo, L. I., Thierry, V., Mercier, H., Bajon, R., & Pérez, F. F. (2024). Anthropogenic carbon pathways towards the North Atlantic interior revealed by Argo-O2, neural networks and back-calculations. *Nature Communications*, *15*(1), 1630. https://doi.org/10.1038/s41467-024-46074-5

Barrett, R. C., Carter, B. R., Fassbender, A. J., Tilbrook, B., Woosley, R. J., Azetsu-Scott, K., Feely, R. A., Goyet, C., Ishii, M., Murata, A., & Pérez, F. F. (2025). Biological Responses to Ocean Acidification Are Changing the Global Ocean Carbon Cycle. *Global Biogeochemical Cycles*, *39*(3), e2024GB008358. https://doi.org/https://doi.org/10.1029/2024GB008358

Berzaghi, F., Pinti, J., Aumont, O., Maury, O., Cosimano, T., & Wisz, M. S. (2025). Global distribution, quantification and valuation of the biological carbon pump. *Nature Climate Change*, *15*(4), 385-392. https://doi.org/10.1038/s41558-025-02295-0

Bindoff, N., Cheung, W. W., Kairo, J., Arstegui, J., Guinder, V., Hallberg, R., Hilmi, N., Jiao, N., Karim, M., & Levin, L. (2019). Changing ocean, marine ecosystems, and dependent communities. In *IPCC special report on the ocean and cryosphere in a changing climate*.

Bittig, H. C., Steinhoff, T., Claustre, H., Fiedler, B., Williams, N. L., Sauzède, R., Körtzinger, A., & Gattuso, J.-P. (2018). An alternative to static climatologies: Robust estimation of open ocean CO2 variables and nutrient concentrations from T, S, and O2 data using Bayesian neural networks. *Frontiers in Marine Science*, *5*, 328.

Bonino, G., Lovecchio, E., Gruber, N., Münnich, M., Masina, S., & Iovino, D. (2021). Drivers and impact of the seasonal variability of the organic carbon offshore transport in the Canary upwelling system. *Biogeosciences*, *18*(8), 2429-2448. https://doi.org/10.5194/bg-18-2429-2021

Boyd, P. W., Claustre, H., Levy, M., Siegel, D. A., & Weber, T. (2019). Multi-faceted particle pumps drive carbon sequestration in the ocean. *Nature*, *568*(7752), 327-335.

Boyd, P. W., Cornwall, C. E., Davison, A., Doney, S. C., Fourquez, M., Hurd, C. L., Lima, I. D., & McMinn, A. (2016). Biological responses to environmental heterogeneity under future ocean conditions. *Global change biology*, *22*(8), 2633-2650.

Boyd, P. W., & Trull, T. W. (2007). Understanding the export of biogenic particles in oceanic waters: Is there consensus? *Progress in Oceanography*, *72*(4), 276-312. https://doi.org/https://doi.org/10.1016/j.pocean.2006.10.007

Burd, A. B., Hansell, D. A., Steinberg, D. K., Anderson, T. R., Arístegui, J., Baltar, F., Beaupré, S. R., Buesseler, K. O., DeHairs, F., & Jackson, G. A. (2010). Assessing the apparent imbalance between geochemical and biochemical indicators of meso-and bathypelagic biological activity: What the@ $♯! is wrong with present calculations of carbon budgets? *Deep Sea Research Part II: Topical Studies in Oceanography*, *57*(16), 1557-1571.

Caesar, L., Rahmstorf, S., Robinson, A., Feulner, G., & Saba, V. (2018). Observed fingerprint of a weakening Atlantic Ocean overturning circulation. *Nature*, *556*(7700), 191-196.

Cavan, E. L., Trimmer, M., Shelley, F., & Sanders, R. (2017). Remineralization of particulate organic carbon in an ocean oxygen minimum zone. *Nature Communications*, *8*(1), 14847. https://doi.org/10.1038/ncomms14847

Chaabane, S., de Garidel-Thoron, T., Meilland, J., Sulpis, O., Chalk, T. B., Brummer, G.-J. A., Mortyn, P. G., Giraud, X., Howa, H., Casajus, N., Kuroyanagi, A., Beaugrand, G., & Schiebel, R. (2024). Migrating is not enough for modern planktonic foraminifera in a changing ocean. *Nature*, *636*(8042), 390-396. https://doi.org/10.1038/s41586-024-08191-5

Ciais, P., Sabine, C., Bala, G., Bopp, L., Brovkin, V., & House, J. I. (2014). Carbon and other biogeochemical cycles. In *Climate Change 2013: The Physical Science Basis. Contribution of Working Group I to the Fifth Assessment Report of the Intergovernmental Panel on Climate Change Change* (pp. 465-570). Cambridge University Press.

Cleveland, W. S. (1979). Robust locally weighted regression and smoothing scatterplots. *Journal of the American statistical association*, *74*(368), 829-836.

Cleveland, W. S., & Devlin, S. J. (1988). Locally weighted regression: an approach to regression analysis by local fitting. *Journal of the American statistical association*, *83*(403), 596-610.

Delaigue, L., Sulpis, O., Reichart, G.-J., & Humphreys, M. P. (2024). The Changing Biological Carbon Pump of the South Atlantic Ocean. *Global Biogeochemical Cycles*, *38*(9), e2024GB008202. https://doi.org/https://doi.org/10.1029/2024GB008202

DeVries, T. (2018). New directions for ocean nutrients. *Nature Geoscience*, *11*(1), 15-16. https://doi.org/10.1038/s41561-017-0042-z

DeVries, T., Primeau, F., & Deutsch, C. (2012). The sequestration efficiency of the biological pump. *Geophysical Research Letters*, *39*(13). https://doi.org/https://doi.org/10.1029/2012GL051963

Dugdale, R., & Goering, J. (1967). Uptake of new and regenerated forms of nitrogen in primary productivity 1. *Limnology and Oceanography*, *12*(2), 196-206.

Falkowski, P., Scholes, R. J., Boyle, E., Canadell, J., Canfield, D., Elser, J., Gruber, N., Hibbard, K., Högberg, P., & Linder, S. (2000). The global carbon cycle: a test of our knowledge of earth as a system. *Science*, *290*(5490), 291-296.

Feely, R. A., Sabine, C. L., Lee, K., Berelson, W., Kleypas, J., Fabry, V. J., & Millero, F. J. (2004). Impact of anthropogenic CO2 on the CaCO3 system in the oceans. *Science*, *305*(5682), 362-366.

Frenger, I., Landolfi, A., Kvale, K., Somes, C. J., Oschlies, A., Yao, W., & Koeve, W. (2024). Misconceptions of the marine biological carbon pump in a changing climate: Thinking outside the "export" box. *Global Change Biology*, *30*(1), e17124. https://doi.org/https://doi.org/10.1111/gcb.17124

Friedlingstein, P., O'Sullivan, M., Jones, M. W., Andrew, R. M., Bakker, D. C. E., Hauck, J., Landschützer, P., Le Quéré, C., Luijkx, I. T., Peters, G. P., Peters, W., Pongratz, J., Schwingshackl, C., Sitch, S., Canadell, J. G., Ciais, P., Jackson, R. B., Alin, S. R., Anthoni, P.,…Zheng, B. (2023). Global Carbon Budget 2023. *Earth Syst. Sci. Data*, *15*(12), 5301-5369. https://doi.org/10.5194/essd-15-5301-2023

Friedlingstein, P., O'Sullivan, M., Jones, M. W., Andrew, R. M., Hauck, J., Landschützer, P., Le Quéré, C., Li, H., Luijkx, I. T., Olsen, A., Peters, G. P., Peters, W., Pongratz, J., Schwingshackl, C., Sitch, S., Canadell, J. G., Ciais, P., Jackson, R. B., Alin, S. R.,…Zeng, J. (2025). Global Carbon Budget 2024. *Earth Syst. Sci. Data*, *17*(3), 965-1039. https://doi.org/10.5194/essd-17-965-2025

Fritsch, F. N., & Carlson, R. E. (1980). Monotone Piecewise Cubic Interpolation. *SIAM Journal on Numerical Analysis*, *17*(2), 238-246. https://doi.org/10.1137/0717021

Fröb, F., Olsen, A., Pérez, F. F., García-Ibáñez, M. I., Jeansson, E., Omar, A., & Lauvset, S. K. (2018). Inorganic carbon and water masses in the Irminger Sea since 1991. *Biogeosciences*, *15*(1), 51-72. https://doi.org/10.5194/bg-15-51-2018

Garcia, H. E., & Gordon, L. I. (1992). Oxygen solubility in seawater: Better fitting equations. *Limnology and Oceanography*, *37*(6), 1307-1312. https://doi.org/https://doi.org/10.4319/lo.1992.37.6.1307

Gruber, N., Bakker, D. C. E., DeVries, T., Gregor, L., Hauck, J., Landschützer, P., McKinley, G. A., & Müller, J. D. (2023). Trends and variability in the ocean carbon sink. *Nature Reviews Earth & Environment*, *4*(2), 119-134. https://doi.org/10.1038/s43017-022-00381-x

Gruber, N., Clement, D., Carter, B. R., Feely, R. A., van Heuven, S., Hoppema, M., Ishii, M., Key, R. M., Kozyr, A., Lauvset, S. K., Lo Monaco, C., Mathis, J. T., Murata, A., Olsen, A., Perez, F. F., Sabine, C. L., Tanhua, T., & Wanninkhof, R. (2019). The oceanic sink

for anthropogenic CO2 from 1994 to 2007. *Science*, *363*(6432), 1193-1199. https://doi.org/10.1126/science.aau5153

Gruber, N., Landschützer, P., & Lovenduski, N. S. (2019). The Variable Southern Ocean Carbon Sink. *Annual Review of Marine Science*, *11*(1), 159-186. https://doi.org/10.1146/annurev-marine-121916-063407

Gruber, N., Sarmiento, J. L., & Stocker, T. F. (1996). An improved method for detecting anthropogenic CO2 in the oceans. *Global Biogeochemical Cycles*, *10*(4), 809-837. https://doi.org/10.1029/96gb01608

Henley, S. F., Cavan, E. L., Fawcett, S. E., Kerr, R., Monteiro, T., Sherrell, R. M., Bowie, A. R., Boyd, P. W., Barnes, D. K. A., Schloss, I. R., Marshall, T., Flynn, R., & Smith, S. (2020). Changing Biogeochemistry of the Southern Ocean and Its Ecosystem Implications [Original Research]. *Frontiers in Marine Science*, *7*. https://doi.org/10.3389/fmars.2020.00581

Henson, S., Le Moigne, F., & Giering, S. (2019). Drivers of carbon export efficiency in the global ocean. *Global Biogeochemical Cycles*, *33*(7), 891-903.

Henson, S. A., Beaulieu, C., & Lampitt, R. (2016). Observing climate change trends in ocean biogeochemistry: when and where. *Global change biology*, *22*(4), 1561-1571.

Henson, S. A., Laufkötter, C., Leung, S., Giering, S. L. C., Palevsky, H. I., & Cavan, E. L. (2022). Uncertain response of ocean biological carbon export in a changing world. *Nature Geoscience*, *15*(4), 248-254. https://doi.org/10.1038/s41561-022-00927-0

Henson, S. A., Sanders, R., Madsen, E., Morris, P. J., Le Moigne, F., & Quartly, G. D. (2011). A reduced estimate of the strength of the ocean's biological carbon pump. *Geophysical Research Letters*, *38*(4).

Holte, J., Talley, L. D., Gilson, J., & Roemmich, D. (2017). An Argo mixed layer climatology and database. *Geophysical Research Letters*, *44*(11), 5618-5626. https://doi.org/https://doi.org/10.1002/2017GL073426

Humphreys, M. P., Griffiths, A. M., Achterberg, E. P., Holliday, N. P., Rérolle, V. M., Menzel Barraqueta, J. L., Couldrey, M. P., Oliver, K. I., Hartman, S. E., & Esposito, M. (2016). Multidecadal accumulation of anthropogenic and remineralized dissolved inorganic carbon along the Extended Ellett Line in the northeast Atlantic Ocean. *Global Biogeochemical Cycles*, *30*(2), 293-310.

Ito, T., Follows, M. J., & Boyle, E. A. (2004). Is AOU a good measure of respiration in the oceans? *Geophysical Research Letters*, *31*(17). https://doi.org/https://doi.org/10.1029/2004GL020900

Jones, D. C., Ito, T., Takano, Y., & Hsu, W. C. (2014). Spatial and seasonal variability of the air-sea equilibration timescale of carbon dioxide. *Global Biogeochemical Cycles*, *28*(11), 1163-1178.

Keppler, L., Landschützer, P., Lauvset, S. K., & Gruber, N. (2023). Recent Trends and Variability in the Oceanic Storage of Dissolved Inorganic Carbon. *Global Biogeochemical Cycles*, *37*(5), e2022GB007677. https://doi.org/https://doi.org/10.1029/2022GB007677

Knuth, D. E. (1969). The art of computer. *Seminumercial Algorithms*, *2*, 268-278.

Koeve, W., Landolfi, A., Oschlies, A., & Frenger, I. (2024). Marine carbon sink dominated by biological pump after temperature overshoot. *Nature Geoscience*, *17*(11), 1093-1099. https://doi.org/10.1038/s41561-024-01541-y

Koseki, S., Crespo, L. R., Tjiputra, J., Fransner, F., Keenlyside, N. S., & Rivas, D. (2024). Assessing the tropical Atlantic biogeochemical processes in the Norwegian Earth System Model. *Biogeosciences*, *21*(18), 4149-4168. https://doi.org/10.5194/bg-21-4149-2024

Kwiatkowski, L., Torres, O., Bopp, L., Aumont, O., Chamberlain, M., Christian, J. R., Dunne, J. P., Gehlen, M., Ilyina, T., John, J. G., Lenton, A., Li, H., Lovenduski, N. S., Orr, J. C., Palmieri, J., Santana-Falcón, Y., Schwinger, J., Séférian, R., Stock, C. A.,…Ziehn, T. (2020). Twenty-first century ocean warming, acidification, deoxygenation, and upper-ocean nutrient and primary production decline from CMIP6 model projections. *Biogeosciences*, *17*(13), 3439-3470. https://doi.org/10.5194/bg-17-3439-2020

Kwon, E. Y., Primeau, F., & Sarmiento, J. L. (2009). The impact of remineralization depth on the air–sea carbon balance. *Nature Geoscience*, *2*(9), 630-635.

Lange, N., Fiedler, B., Álvarez, M., Benoit-Cattin, A., Benway, H., Buttigieg, P. L., Coppola, L., Currie, K., Flecha, S., Gerlach, D. S., Honda, M., Huertas, I. E., Lauvset, S. K., Muller-Karger, F., Körtzinger, A., O'Brien, K. M., Ólafsdóttir, S. R., Pacheco, F. C., Rueda-Roa, D.,…Tanhua, T. (2024). Synthesis Product for Ocean Time Series (SPOTS) – a ship-based biogeochemical pilot. *Earth Syst. Sci. Data*, *16*(4), 1901-1931. https://doi.org/10.5194/essd-16-1901-2024

Laufkötter, C., Vogt, M., Gruber, N., Aumont, O., Bopp, L., Doney, S. C., Dunne, J. P., Hauck, J., John, J. G., & Lima, I. D. (2016). Projected decreases in future marine export production: the role of the carbon flux through the upper ocean ecosystem. *Biogeosciences*, *13*(13), 4023-4047.

Li, G., Cheng, L., Zhu, J., Trenberth, K. E., Mann, M. E., & Abraham, J. P. (2020). Increasing ocean stratification over the past half-century. *Nature Climate Change*, *10*(12), 1116-1123. https://doi.org/10.1038/s41558-020-00918-2

Lønborg, C., Carreira, C., Jickells, T., & Álvarez-Salgado, X. A. (2020). Impacts of Global Change on Ocean Dissolved Organic Carbon (DOC) Cycling [Review]. *Frontiers in Marine Science*, *7*. https://doi.org/10.3389/fmars.2020.00466

Marsay, C. M., Sanders, R. J., Henson, S. A., Pabortsava, K., Achterberg, E. P., & Lampitt, R. S. (2015). Attenuation of sinking particulate organic carbon flux through the mesopelagic ocean. *Proceedings of the National Academy of Sciences*, *112*(4), 1089-1094.

Martin, J. H., Knauer, G. A., Karl, D. M., & Broenkow, W. W. (1987). VERTEX: carbon cycling in the northeast Pacific. *Deep Sea Research Part A. Oceanographic Research Papers*, *34*(2), 267-285.

Masson-Delmotte, V., Zhai, P., Pirani, A., Connors, S., Péan, C., Berger, S., Caud, N., Chen, Y., Goldfarb, L., & Gomis, M. (2021). Contribution of working group I to the sixth assessment report of the intergovernmental panel on climate change. *Climate change*.

Nowicki, M., DeVries, T., & Siegel, D. A. (2022). Quantifying the carbon export and sequestration pathways of the ocean's biological carbon pump. *Global Biogeochemical Cycles*, *36*(3), e2021GB007083.

Nowicki, M., DeVries, T., & Siegel, D. A. (2024). The Influence of Air-Sea CO2 Disequilibrium on Carbon Sequestration by the Ocean's Biological Pump. *Global Biogeochemical Cycles*, *38*(2), e2023GB007880. https://doi.org/https://doi.org/10.1029/2023GB007880

Oschlies, A., Brandt, P., Stramma, L., & Schmidtko, S. (2018). Drivers and mechanisms of ocean deoxygenation. *Nature Geoscience*, *11*(7), 467-473. https://doi.org/10.1038/s41561-018-0152-2

Passow, U., & Carlson, C. A. (2012). The biological pump in a high CO2 world. *Marine Ecology Progress Series*, *470*, 249-271. https://www.int-res.com/abstracts/meps/v470/p249-271/

Pillar, H. R., Hetherington, E., Levin, L. A., Cimoli, L., Lauderdale, J. M., van der Grient, J. M. A., Johannes, K., Heimbach, P., Smith, L., Addey, C. I., Annasawmy, P., Antonio, S., Bax, N., Drake, H. F., Escobar, E., Elsler, L. G., Freilich, M. A., Gallo, N. D., Girard, F.,…Trossman, D. (2024). Future directions for deep ocean climate science and evidence-based decision making [Original Research]. *Frontiers in Climate*, *6*. https://doi.org/10.3389/fclim.2024.1445694

Redfield, A. C. (1958). The biological control of chemical factors in the environment. *American scientist*, *46*(3), 230A-221.

Redfield, A. C. (1963). The influence of organisms on the composition of seawater. *The Sea*, *2*, 26-77. https://ci.nii.ac.jp/naid/10003517839/en/

Ricour, F., Guidi, L., Gehlen, M., DeVries, T., & Legendre, L. (2023). Century-scale carbon sequestration flux throughout the ocean by the biological pump. *Nature Geoscience*, *16*(12), 1105-1113. https://doi.org/10.1038/s41561-023-01318-9

Riebesell, U., Körtzinger, A., & Oschlies, A. (2009). Sensitivities of marine carbon fluxes to ocean change. *Proceedings of the National Academy of Sciences*, *106*(49), 20602-20609. https://doi.org/doi:10.1073/pnas.0813291106

Roemmich, D., & Gilson, J. (2009). The 2004–2008 mean and annual cycle of temperature, salinity, and steric height in the global ocean from the Argo Program. *Progress in Oceanography*, *82*(2), 81-100. https://doi.org/https://doi.org/10.1016/j.pocean.2009.03.004

Sabine, C. L., Feely, R. A., Gruber, N., Key, R. M., Lee, K., Bullister, J. L., Wanninkhof, R., Wong, C. S., Wallace, D. W. R., Tilbrook, B., Millero, F. J., Peng, T.-H., Kozyr, A., Ono, T., & Rios, A. F. (2004). The Oceanic Sink for Anthropogenic CO2. *Science*, *305*(5682), 367-371. https://doi.org/10.1126/science.1097403

Sallée, J.-B., Pellichero, V., Akhoudas, C., Pauthenet, E., Vignes, L., Schmidtko, S., Garabato, A. N., Sutherland, P., & Kuusela, M. (2021). Summertime increases in upper-ocean stratification and mixed-layer depth. *Nature*, *591*(7851), 592-598.

Saunders, P. M., & Fofonoff, N. (1976). Conversion of pressure to depth in the ocean. Deep Sea Research and Oceanographic Abstracts,

Sauzède, R., Bittig, H. C., Claustre, H., Pasqueron de Fommervault, O., Gattuso, J.-P., Legendre, L., & Johnson, K. S. (2017). Estimates of water-column nutrient concentrations and carbonate system parameters in the global ocean: A novel approach based on neural networks. *Frontiers in Marine Science*, *4*, 128.

Schlunegger, S., Rodgers, K. B., Sarmiento, J. L., Frölicher, T. L., Dunne, J. P., Ishii, M., & Slater, R. (2019). Emergence of anthropogenic signals in the ocean carbon cycle. *Nature Climate Change*, *9*(9), 719-725. https://doi.org/10.1038/s41558-019-0553-2

Sharp, J. D., Fassbender, A. J., Carter, B. R., Johnson, G. C., Schultz, C., & Dunne, J. P. (2023). GOBAI-O2: temporally and spatially resolved fields of ocean interior dissolved oxygen over nearly 2 decades. *Earth Syst. Sci. Data*, *15*(10), 4481-4518. https://doi.org/10.5194/essd-15-4481-2023

Siegel, D. A., DeVries, T., Cetinić, I., & Bisson, K. M. (2023). Quantifying the Ocean's Biological Pump and Its Carbon Cycle Impacts on Global Scales. *Annual Review of Marine Science*, *15*(Volume 15, 2023), 329-356. https://doi.org/https://doi.org/10.1146/annurev-marine-040722-115226

Siegenthaler, U., & Sarmiento, J. L. (1993). Atmospheric carbon dioxide and the ocean. *Nature*, *365*(6442), 119-125. https://doi.org/10.1038/365119a0

Sulpis, O., Jeansson, E., Dinauer, A., Lauvset, S. K., & Middelburg, J. J. (2021). Calcium carbonate dissolution patterns in the ocean. *Nature Geoscience*, *14*(6), 423-428.

Sulpis, O., Trossman, D. S., Holzer, M., Jeansson, E., Lauvset, S. K., & Middelburg, J. J. (2023). Respiration Patterns in the Dark Ocean. *Global Biogeochemical Cycles*, *37*(8), e2023GB007747. https://doi.org/https://doi.org/10.1029/2023GB007747

Tjiputra, J. F., Couespel, D., & Sanders, R. (2025). Marine ecosystem role in setting up preindustrial and future climate. *Nature Communications*, *16*(1), 2206. https://doi.org/10.1038/s41467-025-57371-y

Volk, T., & Hoffert, M. I. (1985). Ocean Carbon Pumps: Analysis of Relative Strengths and Efficiencies in Ocean-Driven Atmospheric CO2 Changes. In *The carbon cycle and atmospheric CO2: Natural variations Archean to present* (pp. 99-110). https://doi.org/10.1029/GM032p0099

Walker, S. L., & Palevsky, H. I. (2025). Ocean Carbon Export Flux Projections in CMIP6 Earth System Models Across Multiple Export Depth Horizons. *Global Biogeochemical Cycles*, *39*(4), e2024GB008329. https://doi.org/https://doi.org/10.1029/2024GB008329

Weber, T., Cram, J. A., Leung, S. W., DeVries, T., & Deutsch, C. (2016). Deep ocean nutrients imply large latitudinal variation in particle transfer efficiency. *Proceedings of the National Academy of Sciences*, *113*(31), 8606-8611.

Welch, B. L. (1947). The generalization of 'STUDENT'S'problem when several different population varlances are involved. *Biometrika*, *34*(1-2), 28-35.

Welford, B. P. (1962). Note on a method for calculating corrected sums of squares and products. *Technometrics*, *4*(3), 419-420.

Wilson, J. D., Andrews, O., Katavouta, A., de Melo Viríssimo, F., Death, R. M., Adloff, M., Baker, C. A., Blackledge, B., Goldsworth, F. W., Kennedy-Asser, A. T., Liu, Q., Sieradzan, K. R., Vosper, E., & Ying, R. (2022). The biological carbon pump in CMIP6 models: 21st century trends and uncertainties. *Proceedings of the National Academy of Sciences*, *119*(29), e2204369119. https://doi.org/doi:10.1073/pnas.2204369119

Wunsch, C., & Webb, S. (1979). The climatology of deep ocean internal waves. *Journal of Physical Oceanography*, *9*(2), 235-243.

Yashayaev, I., & Loder, J. W. (2016). Recurrent replenishment of L abrador S ea W ater and associated decadal-scale variability. *Journal of Geophysical Research: Oceans*, *121*(11), 8095-8114.

Zhao, H., Manizza, M., Lozier, M. S., & Cassar, N. (2025). Greener green and bluer blue: Ocean poleward greening over the past two decades. Science, 388(6647), 1337–1340. https://doi.org/10.1126/science.adr9715

Supplementary Files

This is a list of supplementary files associated with this preprint. Click to download.

- DelaigueBCPNGsuppv3.pdf